



HAL
open science

Luminescent N-heterocycles based molecular backbone interleaved within LDH host structure and dispersed into polymer

Paul Legentil, Geneviève Chadeyron, Sandrine Therias, Nicolas Chopin, Doina Sirbu, Franck Suzenet, Fabrice Leroux

► To cite this version:

Paul Legentil, Geneviève Chadeyron, Sandrine Therias, Nicolas Chopin, Doina Sirbu, et al.. Luminescent N-heterocycles based molecular backbone interleaved within LDH host structure and dispersed into polymer. *Applied Clay Science*, 2020, 189, pp.105561. 10.1016/j.clay.2020.105561 . hal-02536944

HAL Id: hal-02536944

<https://hal.science/hal-02536944v1>

Submitted on 20 Nov 2020

HAL is a multi-disciplinary open access archive for the deposit and dissemination of scientific research documents, whether they are published or not. The documents may come from teaching and research institutions in France or abroad, or from public or private research centers.

L'archive ouverte pluridisciplinaire **HAL**, est destinée au dépôt et à la diffusion de documents scientifiques de niveau recherche, publiés ou non, émanant des établissements d'enseignement et de recherche français ou étrangers, des laboratoires publics ou privés.

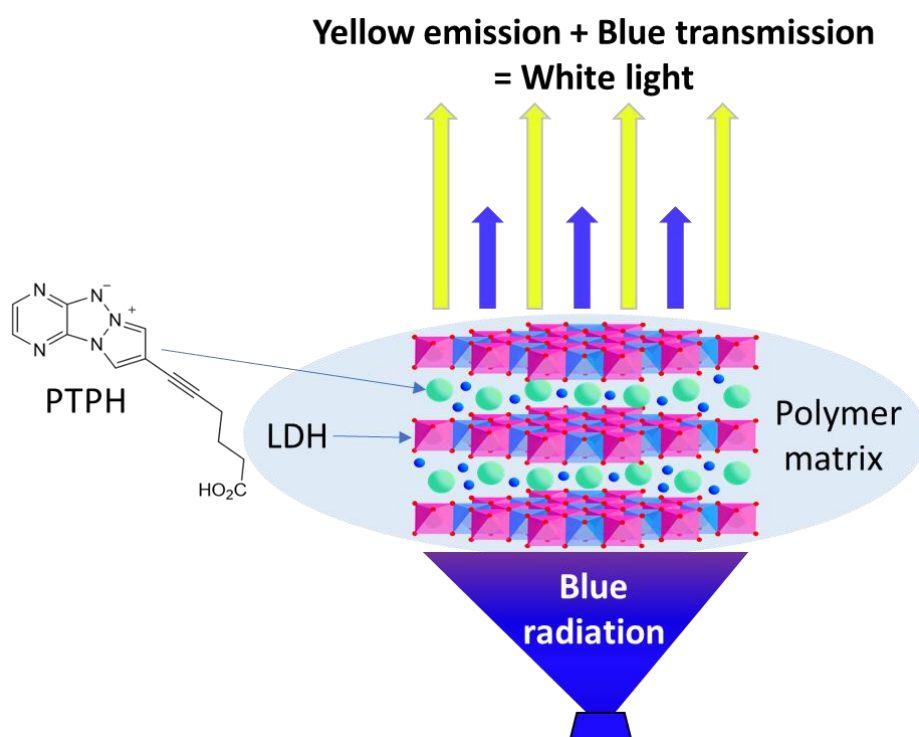
Luminescent N-heterocycles based molecular backbone interleaved into LDH and polymer: for an extensive study

Paul Legentil^a, Geneviève Chadeyron^a, Sandrine Therias^a, Nicolas Chopin^b, Doina Sirbu^b,
Franck Suzenet^b, Fabrice Leroux^{a,*}

^aUniversité Clermont Auvergne, Institut de Chimie de Clermont-Ferrand, UMR CNRS 6296, BP
10448, F-63000 Clermont-Ferrand, France

^bUniversité d'Orléans, Institut de Chimie Organique et Analytique - ICOA UMR CNRS 7311,
Rue de Chartres, F-45100 Orléans, France

Graphical Abstract



11

Highlights

- 12 • Pyrazino-1,3a,6a-triazapentalene dye type structure was intercalated into LDH by co-
13 precipitation method
- 14 • Absolute photoluminescent quantum yields of pristine dye and LDH nanohybrid were
15 compared
- 16 • Luminescent composite films were prepared with the LDH nanohybrid filler
- 17 • Optical properties of the composite films were characterized for potential lighting
18 devices

19 Keywords

20 Layered double hydroxides; Dye; Intercalation; Fluorescence; Composite films.

21 Abstract

22 A pyrazino-1,3a,6a-triazapentalene dye-based molecule was intercalated by direct co-
23 precipitation method into the galleries of negatively charged layered double hydroxide (LDH)
24 to form a new luminescent LDH filler. The materials of cation composition $Zn/Al = 2$ lead to
25 well-defined organic inorganic assemblies. The structure of the hybrid materials was
26 characterized by X-ray diffraction (XRD), Fourier-transform infrared spectra (FTIR) and UV-
27 visible spectra. Optical properties of the materials, at both solid state and slurry state, were
28 also recorded and absolute photoluminescent quantum yields (PLQY) were determined
29 showing that the nanohybrid LDH slurry exhibited higher luminescence properties under UV
30 excitation than the corresponding LDH powder. LDH fillers were used to prepare composite
31 films by dispersion in both hydrophobic or hydrophilic polymer matrix such as poly(dimethyl
32 siloxane) (PDMS) and poly(ethylene oxide) (PEO), respectively. Composite films were

33 characterized by Small Angle X-ray Scattering (SAXS) and PLQY were recorded in order to
34 compare the behaviour of the nanohybrid LDH filler in both polymer matrices. It was found
35 that the aggregation of particles is still observed by SAXS.

36 1. Introduction

37 It is a long-time tradition to use/mix clay minerals with dye molecules, this in particular for
38 coloring used in Egyptian, Maya time, as beautifully exemplified with the famous «blue
39 Maya» as well as for the dye immobilization for water treatment. Both domains were
40 extensively covered with book chapters and reviews (Schoonheydt et al., 2018; Sen, 2017)
41 and are beyond the scope of the present study focusing on advanced sustainable
42 development in lighting devices.

43 It is known that optical properties may inform on the location and accommodation of the
44 guest organic molecule into or onto the clay mineral as recently reported for laponite and
45 fluorescent dye Safranin simply aggregated or built as Langmuir-Blodgett film (Saha et al.,
46 2017).

47 As far as clay mineral and organic dye molecule are concerned, polymer may also play a role
48 in dispersion the aggregated assembly as in polyamide fibers for clothes application using
49 montmorillonite (Mmt) (Almasian et al., 2019) or layered double hydroxide (LDH) with azo-
50 dye (Hajibeygi and Omid-Ghallemohamadi, 2017). Interesting work is also focused on very
51 specific application as those regarding active food packaging polymer, where fluorescent
52 hemicyanine dye-modified Mmt is solvent cast with chitosan to yield bio-nanocomposite
53 films (Mekhzoum et al., 2016).

54 Concerning LDH, their structure is referred to the natural hydrotalcite mineral, and described
55 with the ideal formula, $[M^{II}_{1-x}M^{III}_x(OH)_2] [A^{m-}_{x/m} \cdot nH_2O]$, where M^{II} and M^{III} are metal cations,

56 A^{m-} the interlayered anions, the x value determines the charge density of the LDH and n mol
57 of water molecules per formula weight are also located. Indeed, the isomorphic substitution
58 of M^{II} with M^{III} cations in the brucite-like sheet gives rise to positive electrical charges
59 balanced by exchangeable anions (A^{m-}) leading to the well-known anion exchange/uptake
60 LDH ability.

61 To date, pioneer works conducted by the group of U. Costantino were at first performed to
62 better understand the host / guest interaction and sometimes to address the location of the
63 organic dye, adsorption versus intercalation by scrutinizing the emission fluorescence and
64 the associated emitting state energy coming from the possible interactions between the
65 excited species of the dye molecule and the neighboring unexcited LDH host structure. This
66 was exemplified with azoic dye methyl orange (MO) into LDH (Zn_2Al cation composition) for
67 which the fluorescence of MO interleaved into LDH was found close to MO itself but shifted
68 at higher energies (Costantino et al., 1999), with the xanthene dye fluorescein surface-
69 immobilized or intercalated into LDH (Zn_2Al), where a dual approach using computer
70 modeling and diffuse reflectance experiments helped in describing guest arrangement
71 (Costantino et al., 2000). Their approach was extended to phenolphthalein Zn_2Al hybrid
72 materials for which space-resolved fluorescence imaged the dyes distribution and their
73 interactions with LDH platelets (Latterini et al., 2002), to a series of chromophores,
74 coumarin-3-carboxylic acid (3-CCA), 9-anthracenecarboxylic acid (9-ACA), 4-benzoylbenzoic
75 acid (4-BBA) and 2-naphthalenesulfonic acid (2-NSA) (Aloisi et al., 2002), as well as covering
76 the emerging aspect of fluorescent filler mostly for hydrophobic polymers with anti-
77 microbial and photo-catalytic applications (Costantino et al., 2013) or simply for mechanical
78 reinforcement (Marangoni et al., 2008).

79 After this gain in understanding the interaction between LDH and organic dye molecules,
80 more recent study focus merely on applicative properties such as emphasizing on the
81 tunable photoluminescent film using both fluorescein (FLU) and 1-heptanesulfonic acid
82 sodium (HES) / Zn₂Al hybrid materials for the electro-catalysis of dopamine (Shi et al., 2010).
83 A step further concerns multicolor light-emitting ultrathin films that were built from Mg₂Al
84 LDH hosting photo-functional anions such as bis(N-methylacridinium)@polyvinylsulfonate
85 ion pairs and derivatives of poly(p-phenylene), poly(phenylenevinylene), and
86 poly(thiophene) showing a well-defined multicolor polarized fluorescence in association to
87 high polarization anisotropy thus making them of interest in light displays and optoelectronic
88 devices (Yan et al., 2011). In the same vein, flexible and robust free-standing films including
89 LDH platelets disposed between poly(vinyl alcohol) (PVA) and a styrylbiphenyl derivative
90 (BTBS) via layer-by-layer (LBL) were found to exhibit luminescent anisotropy (Dou et al.,
91 2013).

92 Again, facing new concerns for possible development of optical devices such as to be
93 economic, environmental friendly, rare-earth-free, and to address the life cycle assessment
94 and shelf-life and durability of use, all these prompt us to further study hybrid pigments.

95 These last years, a lot of interest has been carried out to design organic molecules with
96 optical properties for sustainable alternatives of inorganic luminophores, usually composed
97 with rare-earth elements. A lot of organic molecules exhibit very high luminescence property
98 such as N-Heterocyclic compounds and find applications in wide range such as lighting
99 devices (Weber et al., 2015; Zhang et al., 2008), cell imaging sensors (Gogoi and Sen Sarma,
100 2015; Mahajan et al., 2019; Volpi et al., 2018) or even dye-sensitized solar cells (Lu et al.,
101 2018; Wu et al., 2019). Particularly, pyrazino-1,3a,6a-triazapentalene type organic backbone

102 has been identified and substituents are possibly attached to tune the optical properties
103 (antenna effect, shift of the absorption/emission spectra) (Sirbu et al., 2019). In terms of
104 tethering to any host structure, such substituents are the functional groups. Indeed, many
105 researches have proven that both the alkyl chain length and the nature of functional groups
106 could subtly and significantly impact the intermolecular interactions and molecular packing
107 and consequently the optical properties of the dye at solid state or in concentrated solutions
108 (Davis et al., 2008; Kumar et al., 2014). The present study is focus on a dye with a pyrazino-
109 1,3a,6a-triazapentalene based molecular backbone and 5-hexynoic acid as substituent, this
110 dye hereafter called compound "PTPH" in the following. The functionalized antenna of PTPH
111 allows its intercalation within a LDH matrix thanks to the bonds occurring between the
112 hydroxyl layers and the carboxylic acid function. Other substituents are also possible such as
113 formic acid and benzoic acid but the PTPH is the only one which presents luminescence
114 property under solid state. Organic molecules at solid state exhibiting luminescence are very
115 rare. Usual dyes such as fluorescein, eosin or rhodamine form aggregates at solid state
116 responsible of the quenching of luminescence (De et al., 2005; Math et al., 2006).

117 Thus, the dye PTPH has been incorporated into a Zn_2Al LDH matrix by one pot
118 coprecipitation method. The nanohybrid LDH-PTPH was characterised by X-Ray diffraction
119 and FT-IR spectroscopy. The photophysical properties of the pristine dye PTPH and hybrid
120 LDH-PTPH are also scrutinized by UV-visible absorption and fluorescence emission as well as
121 by recording the absolute photoluminescence quantum yield (PLQY). Consequently,
122 composite thin films are prepared by dispersing the LDH-PTPH filler into silicon-type polymer
123 matrix or poly(ethylene oxide). The photophysical properties of the resulting films are also
124 determined in correlation with their morphology analysed by SAXS.

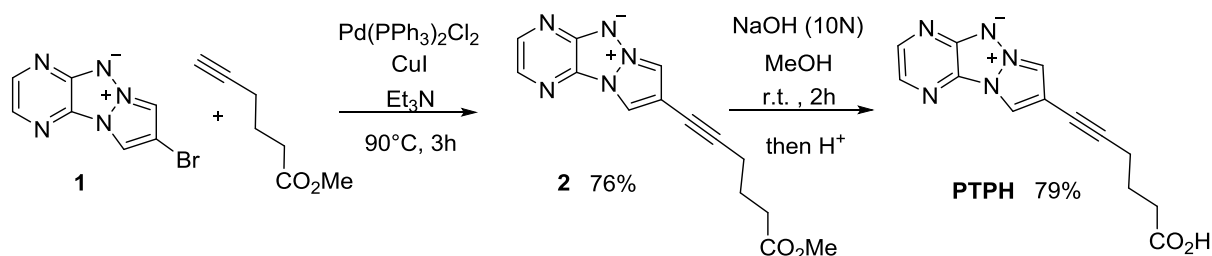
125 2. Materials and Methods

126 2.1. Chemicals

127 The reagents $\text{Zn}(\text{NO}_3)_2 \cdot 6\text{H}_2\text{O}$ (purity 99.9+%), $\text{Al}(\text{NO}_3)_3 \cdot 9\text{H}_2\text{O}$ (purity 99.9+%) and NaOH
128 (97%) were obtained from Sigma Aldrich. The two-component silicon polymer, Bluesil RTV
129 141 part A and part B, were supplied by Elkem. The poly(ethylene oxide) (M_w 100,000 $\text{g}\cdot\text{mol}^{-1}$)
130 ¹) was supplied by Scientific Polymer Products.

131 2.2. Synthesis of PTPH

132 The N-heterocycles dye called PTPH was synthesized starting from the recently reported
133 bromo derivative **1** (Sirbu et al., 2019). For this purpose, compound **1** was first engaged in a
134 Sonogashira cross-coupling reaction with the methyl-5-hexynoate. The resulting ester **2** was
135 then hydrolysed under basic conditions to afford the desired PTPH (Figure 1).



136

137

Figure 1 : Synthesis of PTPH

138 2.3. Synthesis of dye co-intercalated in Zn_2Al LDH

139 The hybrid layered double hydroxide phase, Zn_2Al -Dye, was prepared by the co-precipitation
140 method. The synthesis of $[\text{Zn}_2\text{Al}_1(\text{OH})_6]^+[\text{NO}_3^-]_{1-x}[\text{PTPH}^-]_x \cdot m\text{H}_2\text{O}$, where PTPH^- is the anionic
141 dye, was performed using the target dye in 50 mL of deionized water. 50 mL of an aqueous
142 solution of Zn^{2+} (1.6 mmol) and Al^{+3} (0.8 mmol) was added dropwise during 3 hours under
143 magnetic stirring. For instance, to prepare the sample LDH-PTPH $[\text{Zn}_2\text{Al}_1(\text{OH})_6]^+[\text{NO}_3^-]$
144 $]_{0.60}[\text{PTPH}^-]_{0.4} \cdot m\text{H}_2\text{O}$, 0.32 mmol of the dye was used. The pH was maintained at 9 by adding

145 0.25 M NaOH during all the addition process. The co-precipitation was performed under
146 nitrogen at 20°C. The mixture was centrifuged at 5 000 rpm during 10 minutes; the
147 sedimented solid on the bottom of the flask was washed several times with deionized water
148 until to obtain a clear and transparent supernatant. A paste was recovered and stored at
149 5°C. A small amount was dried over night at room temperature to obtain a powder for
150 further characterizations and to determine the proportion of the dry extract as well as the
151 uptake of PTPH in LDH-(NO₃⁻/PTPH⁻).

152 2.4. Fabrications of composites thin film Silicon/LDH

153 The LDH hybrid powder was used to elaborate the polymer/hybrid material composite with
154 different loadings. The two-component silicone polymer (silicone Bluesil-RTV 141 A&B) was
155 composed of a viscous liquid called part A cured by polyaddition reaction with a catalyser,
156 part B. The silicone film was prepared following the process: a mixture of the part A and 10
157 phr of part B was prepared, homogenised with mechanical mixer (Planetary Centrifugal
158 vacuum Mixer “Thinky Mixer”) during 10 minutes at 500 rpm then pressed in a three rolls
159 mill Exakt 80E. Next, the final composite film was prepared by casting onto a Teflon surface
160 using an Elcometer 4340 automatic film applicator. The blade knife height was fixed at 200
161 µm and the casting speed was 30 mm/s. This two-component silicone polymer was cured at
162 80°C for 2 hours. The film thickness was measured using an Elcometer 456 coating thickness
163 gauge.

164 2.5. Fabrications of composites thin film PEO/LDH

165 The LDH hybrid paste obtained after the last cleaning of LDH-PTPH synthesis was used to
166 elaborate the polymer/hybrid material composite. Hydrophilic poly(ethylene oxide) (PEO)
167 with Mw = 100,000 g.mol⁻¹ was used. 1.0 g of PEO powder was dispersed into 10 mL of

168 deionized water under magnetic stirring during 2 hours. 0.4 g of the LDH-PTPH paste was
169 added to 5.0 g of the previous mixture and then homogenised during 1 hour. The final
170 mixture was poured directly onto a Teflon surface and dried overnight to obtain the
171 composite film PEO-LDH-PTPH.

172 2.6. Techniques of characterization

173 2.6.1. X-ray diffraction

174 LDH powders were characterised by X-Ray Diffraction, the patterns were measured with a
175 Philips X-Pert Pro diffractometer operating with Cu-K α radiation ($\lambda=1.5418 \text{ \AA}$). The data were
176 collected in a 2θ range from 5° to 70° with a step size of $1^\circ/\text{min}$.

177 2.6.2. SAXS

178 Small Angle X-ray Scattering (SAXS) experiments were performed on an Empyrean
179 Panalytical equipment with a ScatterX78 using a θ/θ goniometer and Cu anode (45 kV and 40
180 mA). An elliptic W/Si focusing X-ray mirror for Cu radiation was used, and divergence fixed
181 slit of $1/32^\circ$. The distance from incident beam to sample was 140 mm. The detector
182 GaliPIX3D was at a distance of 240 mm from the sample. SAXS curves were recorded in
183 continuous scan mode. The background (no sample) was removed in each case.

184 2.6.3. Fourier transformed-infrared spectroscopy

185 The infrared spectra were recorded with a Nicolet 5700-FTIR spectrometer with Omnic
186 software. Spectra were obtained using a summation of 32 scans and a resolution of 4 cm^{-1} .
187 Powders of LDH and fluorescein were studied by using the KBr pellet technique.

188 2.6.4. UV-Visible absorption

189 The UV-visible absorption spectra of the samples were recorded in the wavelength range of
190 200 to 800 nm with a UV-vis spectrophotometer (SP-3000 Plus) equipped with an
191 integrating sphere with UV-Probe software.

192 2.6.5. Luminescence

193 Quantum yields efficiencies were measured using an integrating sphere C9920-02G PL-QY
194 measurement system from Hamamatsu Photonics. The setup consisted of a 150 W
195 monochromatized Xe lamp, an integrating sphere (Spectralon coating, $\varnothing=3.3$ in.) and a high
196 sensibility CCD camera. Excitation and blue-excited emission spectra were recorded with a
197 Jobin-Yvon set-up consisting of a Xe lamp operating at 400 W coupled with two
198 monochromators (Triax 550 and Triax 180) and a cryogenically cold charge coupled device
199 (CCD) camera (Jobin-Yvon Symphony LN2 series) for emission spectra and Hamamatsu 980
200 photomultiplier for excitation ones. Excitation spectra were corrected for instrument
201 response and Xe lamp intensity using sodium salicylate. The resolution of the system was
202 better than 0.1 nm in both emission and excitation configurations. Luminescence decays
203 were recorded using a second-harmonic generation on a pulsed Nd:YAG OPO Ekspla NT342A
204 laser (3–5 ns pulse duration, 10 Hz, 5 cm^{-1} line width, 0.3 mJ - 20 mJ in the UV-blue). The
205 emitted photons were detected at right angle from the excitation and analysed through
206 Edinburgh FLS980 spectrometer (Czerny-Turner monochromator, 300 mm focal length, 1200
207 groove mm^{-1} grating and minimum band-pass of 0.1 nm) equipped with Hamamatsu R928P
208 PMT (200–850 nm range).

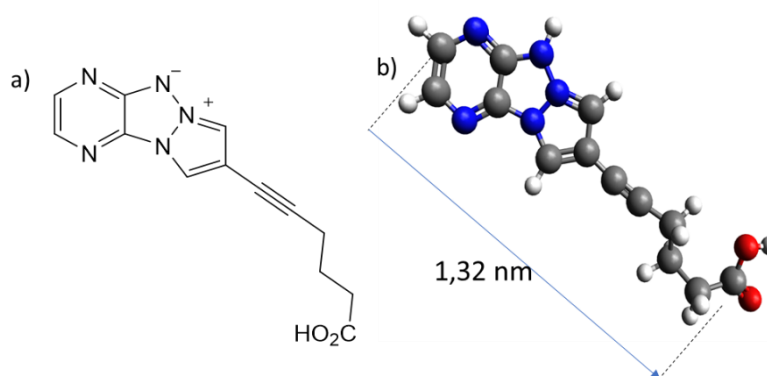
209 2.6.6. Scanning electron microscopy (SEM)

210 Scanning electron microscopy was performed using a ZEISS Supra 55 VP scanning electron
211 microscope in high vacuum, at 20 kV using a back-scatter electron detector (QBSD).

212 3. Results and Discussion

213 3.1. Characterisation of the pristine dyes and the LDH-Dye

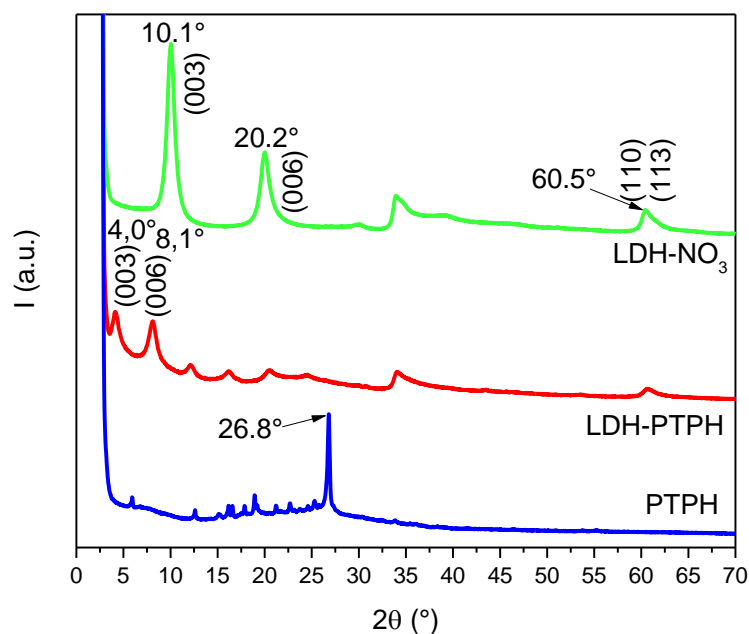
214 The organic molecule PTPH is represented in Figure 2 a). It is composed of a pyrazino-
215 1,3a,6a-triazapentalene molecular backbone with a 4-hexynoic acid substituent chain.
216 Carboxylic acid group is attached to allow the intercalation of the dye molecules between
217 the LDH sheets (Yan et al., 2014). The sample LDH-PTPH powder was synthesized by
218 coprecipitation method. The XRD patterns of LDH-PTPH powder as well as pristine PTPH
219 powder and reference LDH-NO₃ powder where nitrate anions are intercalated in a Zn₂Al LDH
220 matrix, are represented in the Figure 3. Diffraction planes (00 l) are the fingerprints of the
221 layered structure of LDH. For the reference sample LDH-NO₃, the positions of 2 θ = 10.1° and
222 20.2° (i.e. 0.78 nm and 0.39 nm) are characteristic of a nitrate LDH phase and assigned to
223 (003) and (006) diffraction planes, respectively (Mahjoubi et al., 2017). The basal spacing
224 given by the Scherrer equation (Scherrer, 1912) is 0.78 nm for a (003) diffraction plan at a
225 position of 2 θ = 10.1°. (110) and (113) diffraction plans are partially overlapped around 2 θ =
226 60.5° leading to a the metal-to-metal distance within the cationic hydroxide layers of a =
227 $2d_{(110)} = 3.1 \text{ \AA}$, this in agreement with a ratio Zn : Al of 2 : 1 (Vial et al., 2006).



228

229 *Figure 2: a) Molecular structure of the studied dye: a pyrazino-1,3a,6a-triazapentalene type structure; b) 3D molecular*
230 *structure of the dye a with calculated size of the molecule*

231 The diffraction plan (003) and (006) of the XRD pattern of LDH-PTPH are observed at
232 lower 2θ , the peak positions are 4.0° and 8.1° meaning that the basal spacing (2.21 nm) is
233 larger than for the LDH-NO₃ (I. Khan and O'Hare, 2002), thus indicating that the large
234 molecules PTPH are intercalated into the LDH host. Moreover, the geometry of the dye was
235 optimized with Avogadro software and the length of the molecule is estimated to be 1.32
236 nm (Figure 2 b)). The basal spacing agrees well the accommodation of the interleaved dye
237 PTPH. The XRD pattern of the pristine sample PTPH is also represented, a narrow intense
238 peak is observed at $2\theta = 26.8^\circ$ which is not observed for the XRD pattern of LDH-PTPH that
239 excludes the structural packing of free PTPH molecules onto the sample. The mean
240 crystallite size (L) was calculated according to the Scherrer equation $L = k\lambda/(B\cos\theta)$, where B
241 is the full width at half maximum (FWHM) of the diffraction peak (003) and k is the shape
242 factor of the average crystallite and fixed to $k = 0.9$ (assuming a spherical shape) (Cullity,
243 1978). A coherence length L_c along the stacking direction of 17 nm was found for the LDH-
244 PTPH powder meaning that LDH aggregates are composed in average by less than ten
245 stacked layers.



246

247 *Figure 3: X-Ray Diffractogram (XRD) of the pristine dye PTPH and intercalated in a Zn₂Al LDH matrix LDH-PTPH as well as a*
 248 *reference Zn₂Al LDH matrix with nitrate anions intercalated: LDH-NO₃*

249 The FTIR spectra of PTPH and LDH-PTPH recorded between 400 and 4000 cm⁻¹ (Figure 4).

250 Several characteristic bands are observed for the pristine powder PTPH at 1300 cm⁻¹ (C-N

251 aromatic), 1515 cm⁻¹ (C=C aromatic), 1715 cm⁻¹ (stretching bond C=O from carboxylic acid)

252 and around 3100 cm⁻¹ (C-H aromatic). These bands are also visible in the spectra of the LDH-

253 PTPH powder that confirms the presence of PTPH in the sample. However, the IR band at

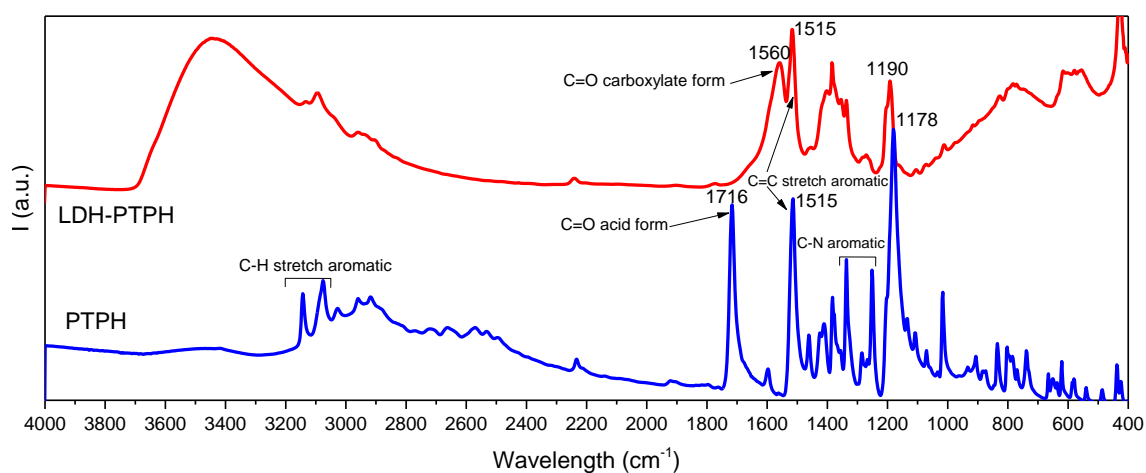
254 1715 cm⁻¹ (stretching bond C-O from carboxylic acid) disappears from the LDH-PTPH IR

255 spectra while a new band appears around 1560 cm⁻¹ which is characteristic of stretching

256 bond C=O from carboxylate. Thus, XRD data as well as FTIR spectra confirm the intercalation

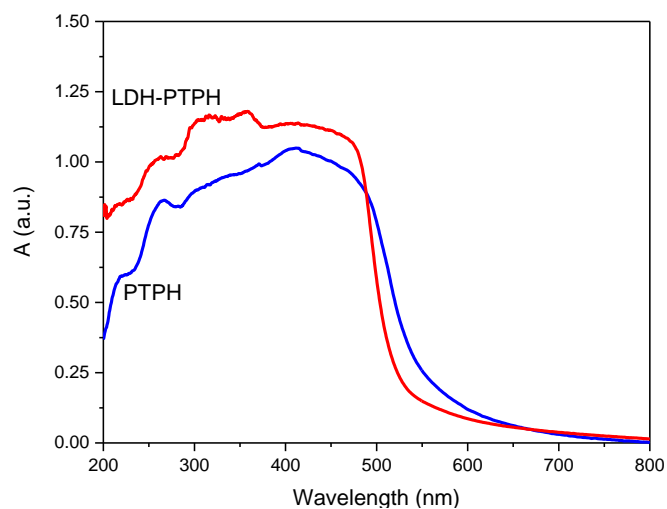
257 and its interaction, respectively, of the molecule PTPH under carboxylate form into the LDH

258 matrix.



259
260 *Figure 4: FTIR spectra of the pristine dye PTPH and intercalated in a Zn₂Al LDH matrix LDH-PTPH recorded into KBr pellets*

261 The UV-Vis absorption spectra of PTPH and LDH-PTPH powders recorded into KBr pellets
262 (Figure 5). Both powders present a large absorbance domain between 200 and 500 nm
263 without a specific absorbance band. The intercalation of PTPH in the LDH matrix does not
264 affect its own absorbance properties.

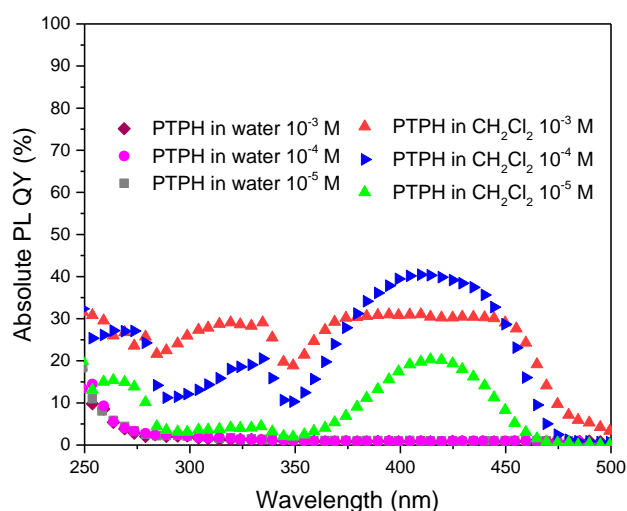


265
266 *Figure 5: UV-visible spectra of the pristine dye PTPH and intercalated in a Zn₂Al LDH matrix LDH-PTPH recorded into KBr*
267 *pellets*

268 3.2. Photoluminescence of the pristine dye and the LDH-Dye

269 The absolute PLQY of the dye recorded between 250 and 500 nm for the compound PTPH in
270 aqueous solution and in dichloromethane solution at three concentrations (10^{-3} , 10^{-4} and 10^{-5}
271 M) is displayed in Figure 6. Thanks to the carboxylate group and the polarity of the dye,
272 PTPH is soluble in water. It is also soluble in organic polar solvent such as dichloromethane

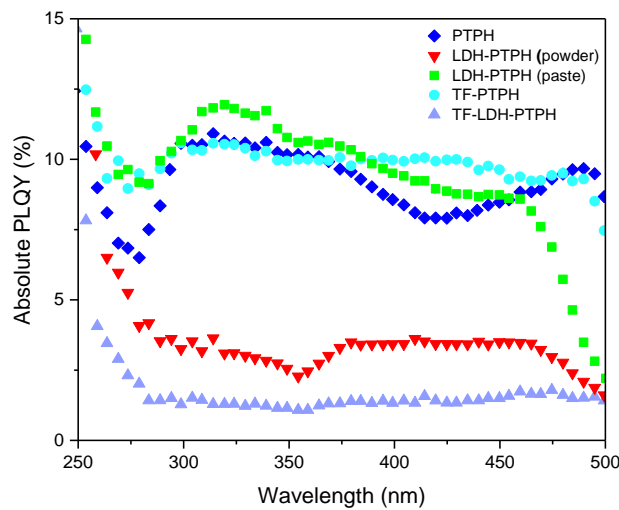
273 or DMSO. The absolute PLQY of PTPH in water is silent; the quenching of luminescence
274 properties occurs whatever the concentration. On the other hand, PTPH in dichloromethane
275 exhibits high absolute PLQY. In a high diluted system (10^{-5} M), PTPH shows absolute PLQY
276 between 340 and 465 nm, the absolute PLQY_{max} is 20.3 % for $\lambda_{\text{exc}} = 315$ nm, whereas the
277 absolute PLQY reaches 40.3 % for 10^{-4} M concentration. At 10^{-3} M, compound PTPH displays
278 a saturation step between 370 and 450 nm due to high concentration.



279
280 *Figure 6: Absolute PLQY in function of the wavelength for solution of PTPH in water and in dichloromethane at three*
281 *different concentration: 10^{-3} , 10^{-4} and 10^{-5} M*

282 The absolute photoluminescence quantum yield (PLQY) of the pristine powder PTPH is
283 illustrated on the Figure 7. The PLQY has been recorded between 250 and 500 nm as if the
284 dye was associated with an UV-LED. The PLQY varies between 6 and 11 % and the maximum
285 is reached at $\lambda_{\text{exc}} = 315$ nm. The values are weak for a potential lighting application but in fact
286 they are very interesting for pristine solid organic dye. Indeed, most of the organic dyes at
287 the solid state such as fluorescein or eosin do not present any luminescent properties at
288 all.(De et al., 2005; De and Kundu, 2011; Yaguchi et al., 2012). The absolute PLQYs of LDH-
289 PTPH under powder and paste form are also reported on the Figure 6. As reported in
290 Experimental section, the paste is obtained after the washing/centrifugation process and
291 before the drying process. The absolute PLQY of the LDH-PTPH powder is almost constant as

292 a function of the wavelength (around 2 %) and are much weaker than the absolute PLQY of
 293 the pristine powder PTPH. Expectedly, the dispersion of the dye into LDH matrix would allow
 294 to reproduce a solid state mixed into a solvated system as in a liquid solution to increase the
 295 absolute PLQY. However, the desired effect is not occurring as for the fluorescein(Legentil et
 296 al., 2019). The absolute PLQY of the LDH-PTPH paste is higher than the absolute PLQY of the
 297 powder, the absolute PLQY_{max} is 11.9 % for $\lambda_{exc} = 320$ nm. Counter intuitively, the paste,
 298 which is just the powder dispersed in a small quantity of water, displays higher absolute
 299 PLQY than the powder, while the luminescence is quenched for PTPH dispersed in water.



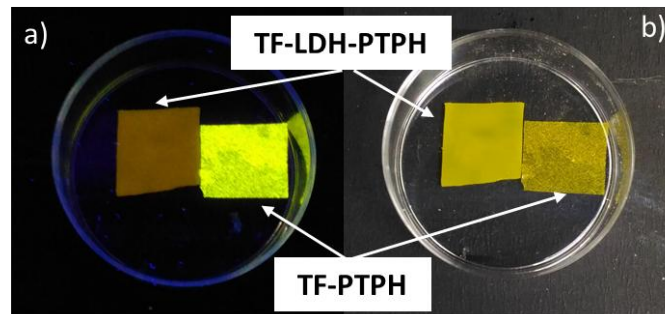
300
 301
 302

Figure 7: Absolute PLQY of powders PTPH and LDH- PTPH as well as paste LDH-PTPH and both composite thin films TF-PTPH and TF-LDH-PTPH

303 3.3. Characterisation of the thin film

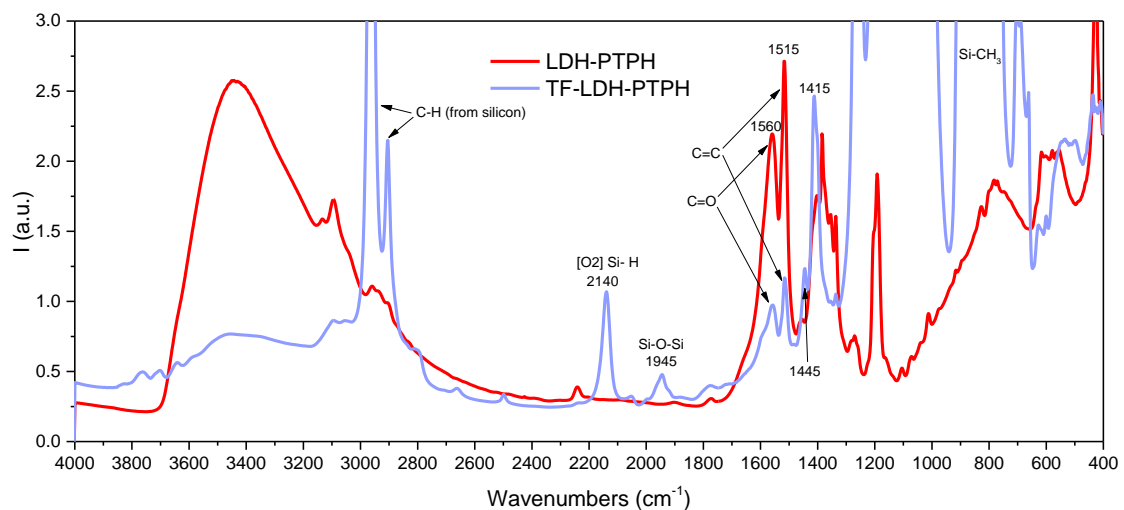
304 Two composite thin films with a silicon matrix (PDMS) was prepared (Deng et al., 2016). The
 305 first one, TF-PTPH, was prepared with pristine powder PTPH with a loading rate of 5 wt. %
 306 whereas the second one, TF-LDH-PTPH, was elaborated with the LDH-PTPH powder with a
 307 loading rate of 20 %_w to get around 5 %_w of PTPH. Both films under UV radiation and under
 308 daylight are illustrated in the Figure 8. First of all, one may observe that the dispersion of
 309 PTPH molecule in the polymer matrix is quite inhomogeneous, as small aggregates are visible
 310 in the thin film TF-PTPH leading to a granular aspect. On the contrary, the dispersion in TF-

311 LDH-PTPH is homogeneous without any aggregates. Thus, LDH matrix has a real additional
312 value in dispersing of the dye PTPH into a polymer matrix. However, TF-PTPH seems to be
313 more luminescent than TF-LDH-PTPH under UV radiation where luminescence is completely
314 turned-off.



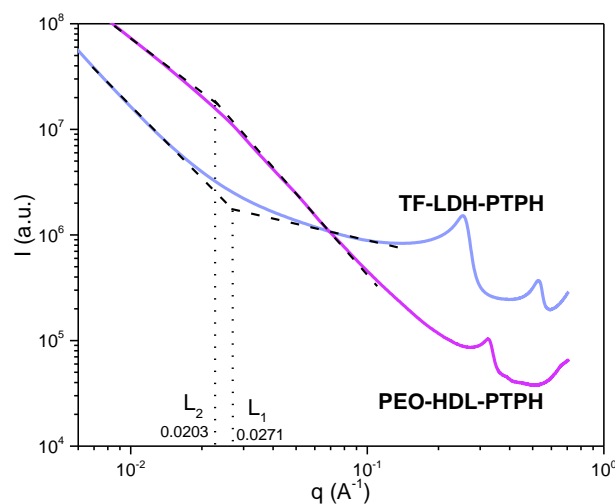
315
316 *Figure 8: Composite thin films of TF-LDH-PTPH and TF-PTPH under daylight and UV irradiation ($\lambda=265$ nm)*

317 The FTIR spectra of LDH-PTPH and TF-LDH-PTPH recorded between 400 and 4000 cm^{-1}
318 (Figure 9). For TF-LDH-PTPH, several IR bands can be attributed to the PDMS polymer (2880-
319 2960, 2140, 1945, 1445, 1415 cm^{-1}) (Bodas and Khan-Malek, 2006). Only two bands, relating
320 to compound PTPH, at 1515 et 1560 cm^{-1} are observed. Thus, the dispersion in the matrix
321 polymer does not modify or degrade the LDH-PTPH powder.



322
323 *Figure 9: FTIR spectra of powder LDH-PTPH recorded into KBr pellets and the composite thin film TF-LDH-PTPH between 400*
324 *and 4000 cm^{-1}*

325 The small-angle X-ray scattering data of both composite films TF-LDH-PTPH and reference
 326 silicon film are presented in Figure 10. Scattered intensity I is plotted versus the scatter
 327 vector q , where $q = 4\pi\sin(\theta)/\lambda$. For TF-LDH-PTPH, a characteristic LDH pattern is observed
 328 (Schaefer and Justice, 2007; Seftel et al., 2015). Two diffraction peaks are observed at 0.26
 329 and 0.53 \AA^{-1} corresponding to distances of 2.42 and 1.18 nm, the first one is the basal
 330 spacing of the LDH matrix. For PEO-HDL-PTPH, only one diffraction peak is observed at 0.33
 331 \AA^{-1} corresponding to a basal spacing of 1.90 nm. These values are closed and match with
 332 data obtained from X-ray diffractogram of the powder LDH-PTPH (2.21 nm). According with
 333 other SAXS investigations (Jarzębski et al., 1997; Tokudome et al., 2016; Wu et al., 2007), the
 334 mean size (L) of secondary aggregated particles, i.e. LDH pellets, can be calculated from the
 335 scatter vector found between the slope modifications of the curve. $L_2 = 27.3 \text{ nm}$ and $L_1 = 23.1$
 336 nm were measured, respectively for TF-LDH-PTPH and for PEO-HDL-PTPH. These values are
 337 slightly higher than the size ($L_c = 17 \text{ nm}$) obtained through the Scherrer equation from the X-
 338 ray diffractogram of the powder HDL-PTPH. It could be explained by a modification of the
 339 environment into the basal spacing or a swelling effect due to the polymer matrices.



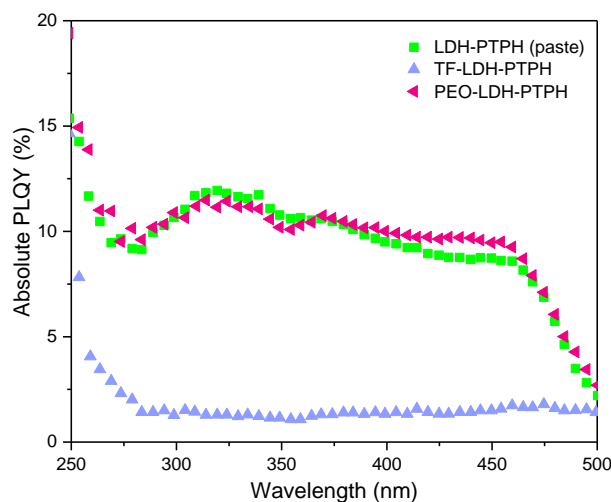
340

341 *Figure 10: Small-angle X Ray scattering (SAXS) of thin composite film TF-LDH-PTPH and a reference silicon film*

342 3.4. Photoluminescence of the thin film

343 The absolute PLQY of both composite films TF-LDH-PTPH and TF-PTPH are presented on
344 Figure 7. The PLQY of TF-PTPH are close to those of the pristine powder PTPH with a
345 maximum of 11 % for $\lambda_{\text{exc}} = 315$ nm. The PLQY of the composite film TF-LDH-PTPH is
346 extremely weak, between 1 and 2 %. The luminescence of the thin film is barely observed
347 under UV irradiation. These results show that the intercalation of the molecule PTPH into
348 LDH host is not suitable for the luminescence properties, this is also the case after dispersion
349 into a PDMS-type polymer.

350 A hydrophilic polymer PEO is then used to prepare a second composite film with the LDH-
351 PTPH paste which presents decent photoluminescence property. The absolute PLQY of the
352 film PEO-LDH-PTPH were presented on Figure 11. The PLQY between 250 and 500 nm are
353 perfectly matching with the PLQY of LDH-PTPH paste. The photoluminescence property of
354 the paste is preserved through its dispersion into a hydrophilic polymer such as PEO, then
355 yielding a luminescent composite film. Further studies are needed to unravel the unexpected
356 behaviour of the observed stable luminescence in such medium.



357
358

Figure 11: Absolute PLQY of composite films PEO-LDH-PTPH and TF-LDH-PTPH as well as paste LDH-PTPH

359 4. Conclusion

360 The study demonstrates that the organic molecule PTPH (pyrazino-1,3a,6a-triazapentalene
361 type structure) exhibits efficient photoluminescence property for an organic molecule at
362 solid state. The cumbersome organic guest PTPH is well intercalated into LDH matrix Zn_2Al
363 using a coprecipitation method, enough ensconced to get a hybrid luminescent material.
364 Counter intuitively, the LDH-PTPH powder does not emit any radiation under blue/UV
365 excitation (absolute PLQY lower than 2 %) whereas the LDH-PTPH paste produces
366 luminescence with an absolute PLQY_{max} of 11.9 % for $\lambda_{exc} = 320$ nm. The dispersion of the
367 LDH-PTPH powder in a polymer (PDMS) occurs readily thanks to the compatible LDH host
368 matrix. However, such dispersion is not able to produce luminescence enough. When
369 hydrophilic polymer such as poly(ethylene oxide) is combined with the LDH-PTPH paste, the
370 absolute PLQY is similar to LDH-PTPH paste values, reaching an absolute PLQY_{max} of 11.5 %
371 for $\lambda_{exc} = 315$ nm, and showing that the continuous phase; i.e. polymer, may play a role at
372 nanoscale.

373 Acknowledgement

374 This work was supported by CPER DEFI MMASYF through its 2016 «MetaProfile» project.
375 Thus, the authors thank European Union in the framework of the European Regional
376 Development Fund (ERDF), and Région Auvergne Rhône-Alpes for the SAXS equipment
377 acquisition and P.L. for his PhD funding « CPER ». In addition, this work was partially
378 supported by Labex SynOrg (ANR-11-LABX-0029), University of Orléans and Région Centre
379 Val de Loire (S2E2 certified OrgaLight project).

- 381 Almasian, A., Mirjalili, M., Maleknia, L., Giahi, M., 2019. Preparation of Multi-Functional Polyester
382 Fabrics with the Use of a New Organo-Clay Nanopigment in High Temperature/High Pressure
383 Condition. *Fibers and Polymers* 20, 1387-1395.
- 384 Aloisi, G.G., Costantino, U., Elisei, F., Latterini, L., Natali, C., Nocchetti, M., 2002. Preparation and
385 photo-physical characterisation of nanocomposites obtained by intercalation and co-
386 intercalation of organic chromophores into hydrotalcite-like compounds. *Journal of Materials*
387 *Chemistry* 12, 3316-3323.
- 388 Bodas, D., Khan-Malek, C., 2006. Formation of more stable hydrophilic surfaces of PDMS by
389 plasma and chemical treatments. *Microelectronic Engineering* 83, 1277-1279.
- 390 Costantino, U., Coletti, N., Nocchetti, M., Aloisi, G.G., Elisei, F., 1999. Anion Exchange of Methyl
391 Orange into Zn-Al Synthetic Hydrotalcite and Photophysical Characterization of the Intercalates
392 Obtained. *Langmuir* 15, 4454-4460.
- 393 Costantino, U., Coletti, N., Nocchetti, M., Aloisi, G.G., Elisei, F., Latterini, L., 2000. Surface Uptake
394 and Intercalation of Fluorescein Anions into Zn-Al-Hydrotalcite. Photophysical Characterization
395 of Materials Obtained. *Langmuir* 16, 10351-10358.
- 396 Costantino, U., Costantino, F., Elisei, F., Latterini, L., Nocchetti, M., 2013. Coupling physical
397 chemical techniques with hydrotalcite-like compounds to exploit their structural features and
398 new multifunctional hybrids with luminescent properties. *Physical Chemistry Chemical Physics*
399 15, 13254-13269.
- 400 Cullity, B.D., 1978. *Elements of X-ray Diffraction*. Addison-Wesley Publishing Company.
- 401 Davis, R., Saleesh Kumar, N.S., Abraham, S., Suresh, C.H., Rath, N.P., Tamaoki, N., Das, S., 2008.
402 Molecular Packing and Solid-State Fluorescence of Alkoxy-Cyano Substituted
403 Diphenylbutadienes: Structure of the Luminescent Aggregates. *The Journal of Physical*
404 *Chemistry C* 112, 2137-2146.
- 405 De, S., Das, S., Girigoswami, A., 2005. Environmental effects on the aggregation of some xanthene
406 dyes used in lasers. *Spectrochimica Acta Part A: Molecular and Biomolecular Spectroscopy* 61,
407 1821-1833.
- 408 De, S., Kundu, R., 2011. Spectroscopic studies with fluorescein dye—Protonation, aggregation
409 and interaction with nanoparticles. *Journal of Photochemistry and Photobiology A: Chemistry*
410 223, 71-81.
- 411 Deng, S., Binauld, S., Mangiante, G., Frances, J.M., Charlot, A., Bernard, J., Zhou, X., Fleury, E., 2016.
412 Microcrystalline cellulose as reinforcing agent in silicone elastomers. *Carbohydrate Polymers*
413 151, 899-906.
- 414 Dou, Y., Liu, X., Shao, M., Han, J., Wei, M., 2013. Flexible and transparent free-standing films with
415 enhanced magnetic and luminescent anisotropy. *Journal of Materials Chemistry A* 1, 4786-4792.
- 416 Gogoi, B., Sen Sarma, N., 2015. Curcumin-cysteine and curcumin-tryptophan conjugate as
417 fluorescence turn on sensors for picric Acid in aqueous media. *ACS applied materials &*
418 *interfaces* 7, 11195-11202.
- 419 Hajibeygi, M., Omid-Ghallemohamadi, M., 2017. One-step synthesized azo-dye modified Mg-Al
420 LDH reinforced biobased semi-aromatic polyamide containing naphthalene ring; study on
421 thermal stability and optical properties. *Journal of Polymer Research* 24, 61.
- 422 I. Khan, A., O'Hare, D., 2002. *Intercalation Chemistry of Layered Double Hydroxides: Recent*
423 *Developments and Applications*.
- 424 Jarzębski, A.B., Lorenc, J., Pająk, L., 1997. Surface Fractal Characteristics of Silica Aerogels.
425 *Langmuir* 13, 1280-1285.
- 426 Kumar, S., Singh, P., Srivastava, R., Koner, R., Pramanik, A., Mathew, J., Sinha, S., Rawat, M., Anand,
427 R., Ghosh, S., 2014. Engineering Fused Coumarin Dyes: Molecular Level Understanding of
428 Aggregation Quenching and Tuning Electroluminescence via Alkyl Chain Substitution.
- 429 Latterini, L., Elisei, F., Aloisi, G.G., Costantino, U., Nocchetti, M., 2002. Space-resolved fluorescence
430 properties of phenolphthalein-hydrotalcite nanocomposites. *Physical Chemistry Chemical*
431 *Physics* 4, 2792-2798.

432 Legentil, P., Leroux, F., Therias, S., Mahiou, R., Chadeyron, G., 2019. Revisiting fluorescein and
433 layered double hydroxide using a synergistic approach: A complete optical study. *Journal of*
434 *Luminescence* 215, 116634.

435 Lu, T.-F., Li, W., Zhang, H.-X., 2018. Rational design of metal-free organic D- π -A dyes in dye-
436 sensitized solar cells: Insight from density functional theory (DFT) and time-dependent DFT
437 (TD-DFT) investigations. *Organic Electronics* 59, 131-139.

438 Mahajan, P.G., Dige, N.C., Vanjare, B.D., Eo, S.-H., Kim, S.J., Lee, K.H., 2019. A nano sensor for
439 sensitive and selective detection of Cu²⁺ based on fluorescein: Cell imaging and drinking water
440 analysis. *Spectrochimica Acta Part A: Molecular and Biomolecular Spectroscopy* 216, 105-116.

441 Mahjoubi, F.Z., Khalidi, A., Abdennouri, M., Barka, N., 2017. Zn-Al layered double hydroxides
442 intercalated with carbonate, nitrate, chloride and sulphate ions: Synthesis, characterisation and
443 dye removal properties. *Journal of Taibah University for Science* 11, 90-100.

444 Marangoni, R., Taviot-Guého, C., Illaik, A., Wypych, F., Leroux, F., 2008. Organic inorganic dye
445 filler for polymer: Blue-coloured layered double hydroxides into polystyrene. *Journal of Colloid*
446 *and Interface Science* 326, 366-373.

447 Math, N.N., Naik, L.R., Suresh, H.M., Inamdar, S.R., 2006. Dual fluorescence and laser emissions
448 from fluorescein-Na and eosin-B. *Journal of Luminescence* 121, 475-487.

449 Mekhzoum, M.E.M., Essassi, E.M., Qaiss, A., Bouhfid, R., 2016. Fluorescent bio-nanocomposites
450 based on chitosan reinforced hemicyanine dye-modified montmorillonite. *RSC Advances* 6,
451 111472-111481.

452 Saha, M., Shil, A., Hussain, S.A., Bhattacharjee, D., 2017. Clay induced changes in the aggregation
453 pattern of Safranin-O in hybrid Langmuir-Blodgett (LB) films. *Journal of Photochemistry and*
454 *Photobiology A: Chemistry* 348, 199-208.

455 Schaefer, D.W., Justice, R.S., 2007. How Nano Are Nanocomposites? *Macromolecules* 40, 8501-
456 8517.

457 Scherrer, P., 1912. Bestimmung der inneren Struktur und der Größe von Kolloidteilchen mittels
458 Röntgenstrahlen, *Kolloidchemie Ein Lehrbuch*. Springer Berlin Heidelberg, Berlin, Heidelberg,
459 pp. 387-409.

460 Schoonheydt, R., Johnston, C.T., Bergaya, F., 2018. Surface and interface chemistry of clay
461 minerals.

462 Seftel, E., Niarchos, M., Vordos, N., Nolan, J., Mertens, M., Mitropoulos, A.C., Vansant, E., Cool, P.,
463 2015. LDH and TiO₂/LDH-type nanocomposite systems: A systematic study on structural
464 characteristics.

465 Sen, T.K., 2017. Clay minerals : properties, occurrence, and uses. Nova Science Publishers.

466 Shi, W., Sun, Z., Wei, M., Evans, D.G., Duan, X., 2010. Tunable Photoluminescence Properties of
467 Fluorescein in a Layered Double Hydroxide Matrix by Changing the Interlayer
468 Microenvironment. *The Journal of Physical Chemistry C* 114, 21070-21076.

469 Sirbu, D., Diharce, J., Martinić, I., Chopin, N., Eliseeva, S.V., Guillaumet, G., Petoud, S., Bonnet, P.,
470 Suzenet, F., 2019. An original class of small sized molecules as versatile fluorescent probes for
471 cellular imaging. *Chemical communications* 55, 7776-7779.

472 Tokudome, Y., Morimoto, T., Tarutani, N., Vaz, P.D., Nunes, C.D., Prevot, V., Stenning, G.B.G.,
473 Takahashi, M., 2016. Layered Double Hydroxide Nanoclusters: Aqueous, Concentrated, Stable,
474 and Catalytically Active Colloids toward Green Chemistry. *ACS Nano* 10, 5550-5559.

475 Vial, S., Ghanbaja, J., Forano, C., 2006. Precipitation of Zn₂Al LDH by urease enzyme. *Chemical*
476 *communications*, 290-292.

477 Volpi, G., Lace, B., Garino, C., Priola, E., Artuso, E., Cerreia Vioglio, P., Barolo, C., Fin, A., Genre, A.,
478 Prandi, C., 2018. New substituted imidazo[1,5-a]pyridine and imidazo[5,1-a]isoquinoline
479 derivatives and their application in fluorescence cell imaging. *Dyes and Pigments* 157, 298-304.

480 Weber, M.D., Niklaus, L., Proschel, M., Coto, P.B., Sonnewald, U., Costa, R.D., 2015. Bioinspired
481 Hybrid White Light-Emitting Diodes. *Advanced materials* 27, 5493-5498.

482 Wu, H., Huang, Z., Hua, T., Liao, C., Meier, H., Tang, H., Wang, L., Cao, D., 2019. Metal-free organic
483 dyes with di(1-benzothieno)[3,2-b:2',3'-d]pyrrole as a donor for efficient dye-sensitized solar
484 cells: Effect of mono- and bi-anchors on photovoltaic performance. *Dyes and Pigments* 165, 103-
485 111.

486 Wu, Q., Sjøstad, A.O., Vistad, Ø.B., Knudsen, K.D., Roots, J., Pedersen, J.S., Norby, P., 2007.
487 Characterization of exfoliated layered double hydroxide (LDH, Mg/Al = 3) nanosheets at high
488 concentrations in formamide. *Journal of Materials Chemistry* 17, 965-971.
489 Yaguchi, K., Furube, A., Katoh, R., 2012. Aggregate formation of eosin-Y adsorbed on
490 nanocrystalline TiO₂ films. *Chemical Physics Letters* 551, 96-100.
491 Yan, D., Lu, J., Wei, M., Qin, S., Chen, L., Zhang, S., Evans, D.G., Duan, X., 2011. Heterogeneous
492 Transparent Ultrathin Films with Tunable-Color Luminescence Based on the Assembly of
493 Photoactive Organic Molecules and Layered Double Hydroxides. *Advanced Functional Materials*
494 21, 2497-2505.
495 Yan, L., Wang, Y., Li, J., Kalytchuk, S., Susha, A.S., Kershaw, S.V., Yan, F., Rogach, A.L., Chen, X.,
496 2014. Highly luminescent covalently bonded layered double hydroxide-fluorescent dye
497 nanohybrids. *Journal of Materials Chemistry C* 2, 4490.
498 Zhang, L., Li, B., Lei, B., Hong, Z., Li, W., 2008. A triphenylamine derivative as an efficient organic
499 light color-conversion material for white LEDs. *Journal of Luminescence* 128, 67-73.

500

501

502

503

Supporting information

504

505 **Materials and methods**

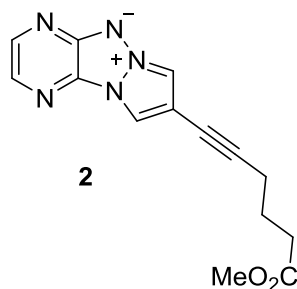
506 Nuclear Magnetic Resonance (NMR) spectra were recorded on a 250 or 400 MHz
507 Bruker NMR spectrometers in CDCl₃ or DMSO. All chemical shift values are reported in parts
508 per million (ppm) with coupling constant (J) values reported in Hz. All spectra were
509 referenced to the CDCl₃ residual solvent peak CHCl₃ (δ = 7.26 ppm) for ¹H NMR and the CDCl₃
510 solvent peak (δ = 77.16 ppm) for ¹³C NMR. The notation of signals is: Proton: δ chemical shift
511 in ppm (multiplicity, J value(s), number of protons). Carbon: δ chemical shift in ppm.
512 Fluorine: δ chemical shift in ppm. Splitting patterns are assigned s = singlet, b = broad, d =
513 doublet, td = triplet of doublet, dt = doublet of triplet, t = triplet, q = quartet, app= apparent.

514

515 All reaction were monitored by thin-layer chromatography (TLC) analysis using silica
516 gel (60 F254). Solvents, unless otherwise stated, were purchased in reagent grade or
517 anhydrous quality and used as received. Reagents were either purchased directly from
518 commercial suppliers or prepared according to literature procedures. Yields of all the
519 compounds refer to isolated compounds. Chromatography: Separations were carried out on
520 Silica gel 60, (40-63 μ , 60 Å) purchased from Sigma Aldrich. High Resolution Mass
521 Spectrometry (HRMS) were recorded on Maxis Bruker 4G. Melting points (mp [C°]) were
522 taken on open capillary tubes using a Electrothermal IA 9100 apparatus.

523 Reactants were purchased from commercial suppliers and were used without further
524 purification. Compound **1** was synthesized following reported synthesis (Sirbu et al., 2019).

525 Experimental procedures



526

527 In a round bottom flask, the bromopyridazinotriazapentalene **1** (Sirbu et al., 2019) (1.0 g,
528 4.20 mmol) was solubilized in Et₃N (10 mL) with methyl-5-hexynoate (1.060 g, 8.40 mmol, 2
529 eq.) and Pd(PPh₃)₂Cl₂ (294.8 mg, 0.42 mmol, 10 mol%). The mixture was stirred at room
530 temperature for 20 min and then CuI (72.4 mg, 0.38 mmol, 9 mol%) was added. The mixture
531 was stirred at 90°C for 3h. Solvent was removed under vacuum and crude compound purified
532 by column chromatography (DCM/AcOEt 1/1) to give pure **2** (900 mg, 76%) as a yellow solid.

533 Pf: 99°C

534 IR $\nu(\text{cm}^{-1})$: 3138, 3078, 2959, 1721, 1507, 1424, 1382, 1368, 1336, 1256, 1186.

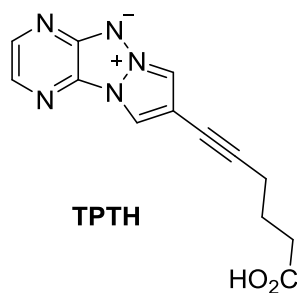
535 ¹H NMR (400 MHz, Chloroform-d) δ 8.35 (d, $J = 2.7$ Hz, 1H), 8.03 (s, 1H), 7.83 (d, $J = 2.7$ Hz,
536 1H), 7.78 (s, 1H), 3.63 (s, 3H), 2.45 (td, $J = 7.2, 5.4$ Hz, 4H), 1.89 (p, $J = 7.2$ Hz, 2H).

537 ¹³C NMR (101 MHz, CDCl₃) δ 173.27, 152.43, 143.33, 130.43, 128.94, 111.86, 110.52, 107.83,
538 93.28, 70.19, 51.66, 32.81, 23.49, 18.86.

539 HRMS (ESI) m/z : calculated for C₁₄H₁₄N₅O₂ [M+H]⁺ 284.1142; found 284.1141.

540

541



542

543 In a round bottom flask, **2** (500 mg, 1.77 mmol) was solubilized in MeOH (4 mL) with NaOH
544 10N (1 mL, 10 mmol, 5.6 eq.). The mixture was stirred at room temperature for 2h. Solvents
545 were removed under vacuum and the crude mixture solubilized in DCM and water (1/1).
546 Aqueous phase was extracted and washed with DCM (3 x 20 mL) and then acidified with HCl
547 2N until pH 4-5. Organic phase was extracted with DCM, washed with water and
548 concentrated under vacuum to give pure **TPTH** (377 mg, 1.40 mmol, 79%).

549 *Pf*: ~175°C (decomp.)

550 IR $\nu(\text{cm}^{-1})$: 3143, 3074, 2960, 1715, 1512, 1382, 1336, 1250, 1176, 1016.

551 ^1H NMR (400 MHz, DMSO- d_6) δ 12.14 (s, 1H), 8.85 (s, 1H), 8.58 (s, 1H), 8.36 (d, J = 2.7 Hz,
552 1H), 7.90 (d, J = 2.7 Hz, 1H), 2.55 – 2.46 (m, 2H), 2.38 (t, J = 7.3 Hz, 2H), 1.78 (p, J = 7.2 Hz,
553 2H).

554 ^{13}C NMR (101 MHz, DMSO) δ 173.96, 152.08, 142.65, 129.59, 128.92, 113.90, 111.37,
555 106.68, 92.99, 70.80, 32.60, 23.46, 18.16.

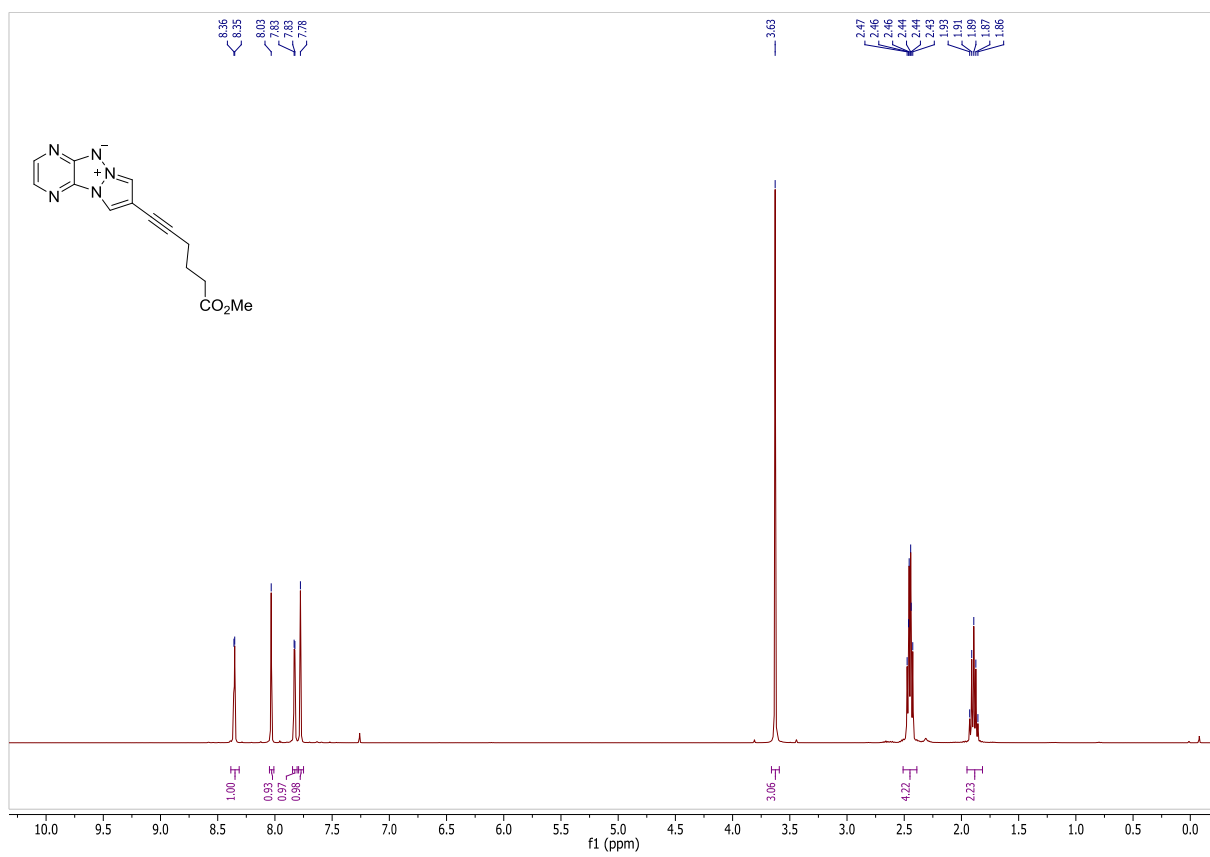
556 HRMS (ESI) m/z : calculated for $\text{C}_{13}\text{H}_{12}\text{N}_5\text{O}_2$ $[\text{M}+\text{H}]^+$ 270.0985; found 270.0984.

557

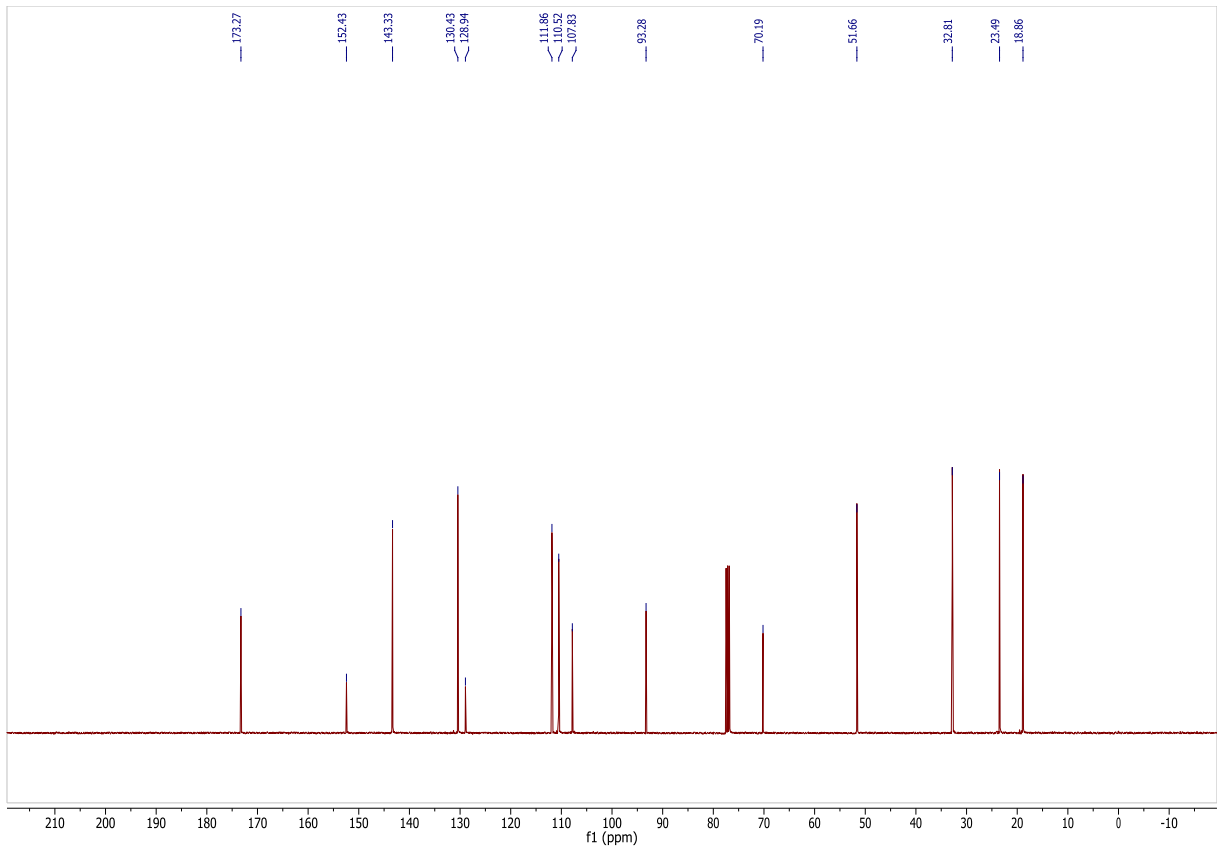
558

559

560 NMR spectra

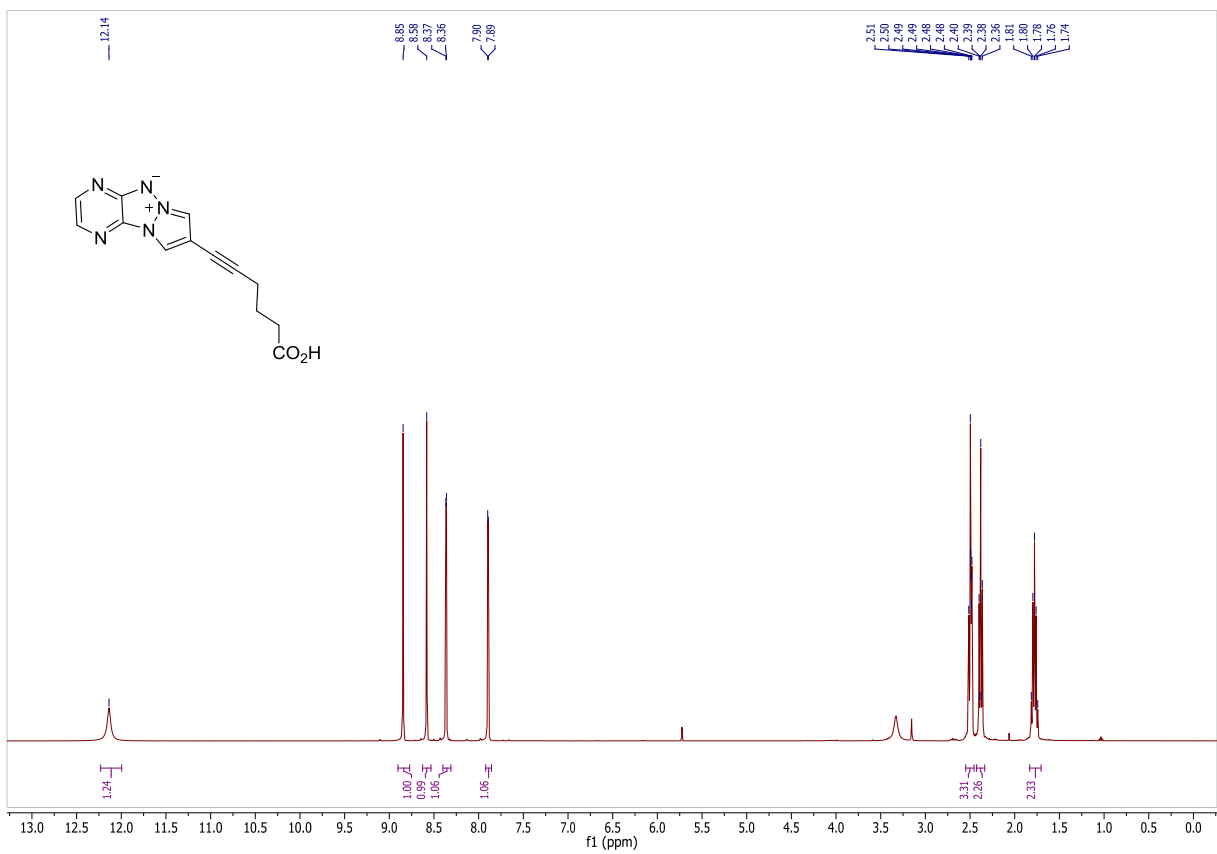


561



562

563



564

565

